

RGC-specific ATF4 and/or CHOP deletion rescues glaucomatous neurodegeneration and visual function

Fang Fang,^{1,3} Pingting Liu,¹ Haoliang Huang,¹ Xue Feng,¹ Liang Li,¹ Yang Sun,¹ Randal J. Kaufman,² and Yang Hu¹

¹Department of Ophthalmology, Stanford University School of Medicine, Palo Alto, CA 94304, USA; ²Degenerative Diseases Program, Center for Genetic Disorders and Aging Research, Sanford Burnham Prebys Medical Discovery Institute, La Jolla, CA 92037, USA; ³Department of Ophthalmology, The Second Xiangya Hospital, Central South University, Changsha 410011, China

Endoplasmic reticulum (ER) stress has been linked with various acute and chronic neurodegenerative diseases. We previously found that optic nerve (ON) injury and diseases induce neuronal ER stress in retinal ganglion cells (RGCs). We further demonstrated that germline deletion of CHOP preserves the structure and function of both RGC somata and axons in mouse glaucoma models. Here we report that RGC-specific deletion of CHOP and/or its upstream regulator ATF4 synergistically promotes RGC and ON survival and preserves visual function in mouse ON crush and silicone oil-induced ocular hypertension (SOHU) glaucoma models. Consistently, topical application of the ATF4/CHOP chemical inhibitor ISRIB or RGC-specific CRISPR-mediated knockdown of the ATF4 downstream effector Gadd45a also delivers significant neuroprotection in the SOHU glaucoma model. These studies suggest that blocking the neuronal intrinsic ATF4/CHOP axis of ER stress is a promising neuroprotection strategy for neurodegeneration.

INTRODUCTION

When the endoplasmic reticulum (ER) is overwhelmed by misfolded proteins or disturbed calcium homeostasis, cells experience ER stress and activate a complex cascade of reactions, in general called the unfolded protein response (UPR).^{1,2} ER stress is linked with various acute and chronic neurodegenerative diseases.^{3–5} Modulation of ER stress and UPR signaling molecules protects injured neurons and improves functional recovery in experimental spinal cord injury,^{6–10} stroke,^{11–13} Alzheimer's disease (AD),^{14,15} Parkinson's disease (PD),^{16,17} amyotrophic lateral sclerosis (ALS),¹⁸ prion disease,^{19–21} and retina degenerations.^{22–27} We previously found that traumatic optic nerve (ON) injury, ocular hypertension, and optic neuritis induce neuronal ER stress in retinal ganglion cells (RGCs).^{28–30} We further demonstrated that germline knockout (KO) of CHOP, a downstream pro-apoptotic molecule of ER stress,^{31–33} or treatment with small molecular CHOP inhibitors, preserves the structure and function of both RGC somata and axons in several mouse optic neuropathy models.^{28–30,34} These findings indicate the critical importance of ER stress in the pathophysiology of axonopathies and that inhibition of the CHOP branch of ER stress is a promising neuroprotection strategy.^{3,35}

CHOP mediates ER stress-induced apoptosis by downregulating anti-apoptotic Bcl2³⁶ and upregulating pro-apoptotic Bim and PUMA,^{37,38} death receptor 5 (DR5), and caspase 8 cleavage.³⁹ CHOP also can form heterodimers with its upstream transcription factor ATF4 to cause cell death by upregulating protein synthesis and inducing oxidative stress.⁴⁰ Axonal ATF4 was linked to AD pathogenesis,⁴¹ and ATF4 activation promotes dopaminergic cell death induced by PD neurotoxins and pathogenic α -synuclein aggregates.⁴² It is clinically important and scientifically interesting to determine the role of neuronal specific ATF4/CHOP inhibition in neuroprotection. The Cre-dependent CHOP floxed mouse line and ATF4 floxed mouse line have been generated for cell-type-specific testing.^{43,44} Taking advantage of our recently developed RGC-specific AAV promoter, mouse γ -synuclein (mSncg)⁴⁵ and silicone oil-induced ocular hypertension (SOHU) mouse glaucoma models,^{46–48} we demonstrate here that RGC-specific deletion of CHOP, ATF4, or both significantly preserves glaucomatous RGC somata and axons and visual function. Consistently, ISRIB, a small molecule inhibitor of the ATF4/CHOP axis, and CRISPR-mediated knock down of Gadd45a, a potential ATF4 downstream effector, also provide neuroprotection in the mouse glaucoma model. This study confirms that targeting the neuronal intrinsic ATF4-CHOP axis of ER stress is a promising neuroprotective strategy.

RESULTS

RGC-specific deletion of ATF4 and/or CHOP promotes significant RGC soma and axon survival after ON crush injury

To test the effect of neuronal intrinsic inhibition of ATF4 and/or CHOP, we employed CHOP floxed mice⁴³ and ATF4 floxed mice,⁴⁴ and we generated an ATF4/CHOP double-floxed mouse line. Because endogenous levels of ATF4 and CHOP in naive RGCs are quite low, it is difficult to detect the KO effect in the naive transgenic mouse lines. ON crush (ONC) induced upregulation of ATF4 and CHOP in injured RGCs at 3 days post crush (3dpc)²⁸ (Figures 1A and 1B), and

Received 20 January 2023; accepted 11 July 2023;
<https://doi.org/10.1016/j.omtn.2023.07.015>.

Correspondence: Yang Hu, Department of Ophthalmology, Stanford University School of Medicine, Palo Alto, CA 94304, USA.

E-mail: huyang@stanford.edu

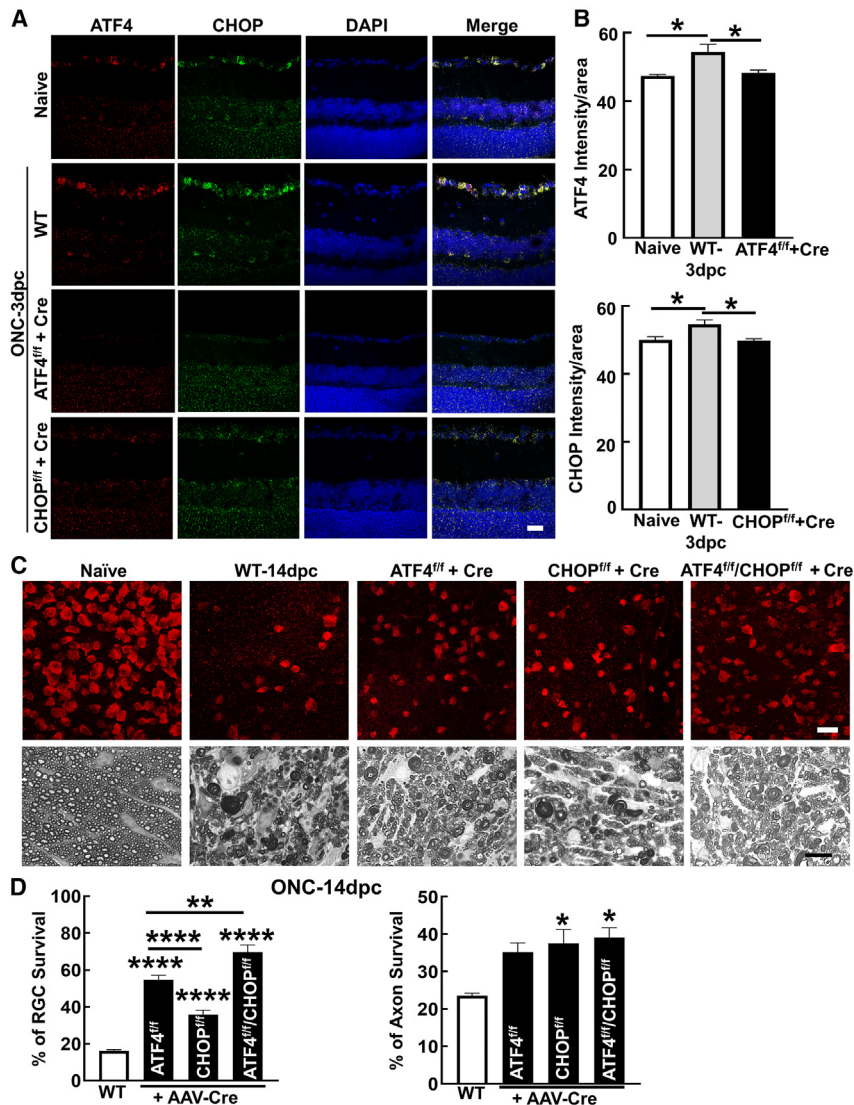


Figure 1. ATF4 and/or CHOP deletion promotes RGC soma and axon survival in ONC model

(A) Representative confocal images of retina cross-sections showing ATF4 (red) and CHOP (green) mRNA expression in GCL by ISH at 3dpc (days post crush) in WT, ATF4, or CHOP KO mice. GCL, ganglion cell layer; ISH, *in situ* hybridization. Scale bar, 20 μ m. (B) Quantification of mean fluorescence intensity of ATF4 and CHOP in GCL at 3dpc. $n = 5$ in all groups. Data are presented as means \pm SEM. * $p < 0.05$, one-way ANOVA with Tukey's multiple comparisons test. (C) Upper panel, representative confocal images of peripheral flat-mounted retinas showing surviving RBPMS-positive (red) RGCs at 14dpc. Scale bar, 20 μ m. Lower panel, light microscope images of semi-thin transverse sections of ON with PPD staining at 14dpc. Scale bar, 10 μ m. (D) Quantification of surviving RGC somata and axons at 14dpc, represented as percentage of crushed eyes compared to the sham contralateral control eyes. WT, $n = 10$; ATF4^{fl/fl}, $n = 6$; CHOP^{fl/fl}, $n = 9$; and ATF4^{fl/fl}/CHOP^{fl/fl}, $n = 7$. Data are presented as means \pm SEM, ** $p < 0.01$, **** $p < 0.0001$, one-way ANOVA with Tukey's multiple comparisons test.

intravitreal injection of AAV2-Cre driven by RGC-specific promoter mSncg⁴⁵ in ATF4- and CHOP-floxed mice (Figure S1A) significantly inhibited ATF4 and CHOP expression in injured RGCs (Figures 1A and 1B). Consistently, RGC-specific ATF4 or CHOP deletion significantly increased RGC soma survival after ONC injury (Figures 1C, 1D, and S1B). Interestingly, ATF4 KO provided greater RGC protection than CHOP KO, and ATF4/CHOP double KO was more effective than either one alone. RGC-specific deletion of CHOP or both ATF4 and CHOP also protected RGC axons, although axon protection by ATF4 KO did not reach statistical significance (Figures 1C and 1D).

RGC-specific deletion of ATF4 and/or CHOP significantly promotes both RGC soma and axon survival in the SOHU glaucoma model

Next, we tested the RGC autonomous effect of ATF4/CHOP deletion in a mouse glaucoma model (Figure S1B). We generated the SOHU glau-

coma model in one eye and used the contralateral eye as naive control.^{46–48} ATF4 and CHOP upregulation was readily detected in the SOHU eyes 1 week post silicone oil (SO) injection (1wpi) (Figures 2A and 2B). ATF4 or CHOP deletion in RGCs did not affect intraocular pressure (IOP) elevation (Figure 2C). Optokinetic tracking response (OKR) is a natural reflex that objectively assesses mouse visual acuity.^{49,50} Deletion of ATF4, CHOP, or both in RGCs significantly preserved visual acuity of the glaucomatous eyes 3 weeks post SO injection (3wpi) (Figure 2D). A common RGC electrophysiological assay, pattern electroretinogram (PERG), consistently showed significant increase of the peak-to-trough (P1-N2) amplitude ratio of the SOHU eyes to contralateral (CL) eyes after ATF4/CHOP KO (Figure 2E), also indicating improved visual function.

In addition to *in vivo* visual function assessment, we also performed *in vivo* OCT imaging of mouse retinas and found that RGC-specific KO of ATF4, CHOP, or both significantly increased the thickness of the ganglion cell complex (GCC), including both RGC dendrites and axons, in glaucoma eyes (Figures 2F and 2G). Histological analysis of postmortem retina whole mounts (Figure S2A) and ON sections (Figure S2E) consistently demonstrated significant increase of RGC somata and axons in SOHU eyes after deletion of ATF4, CHOP, or both in RGCs (Figures 3 and S2B–S2D). Although there was no statistically significant difference in glaucoma neuroprotection among the groups of RGC-specific manipulation, ATF4/CHOP double KO consistently showed better effects. Taken together, these results indicate that RGC-specific inhibition of ATF4 and CHOP

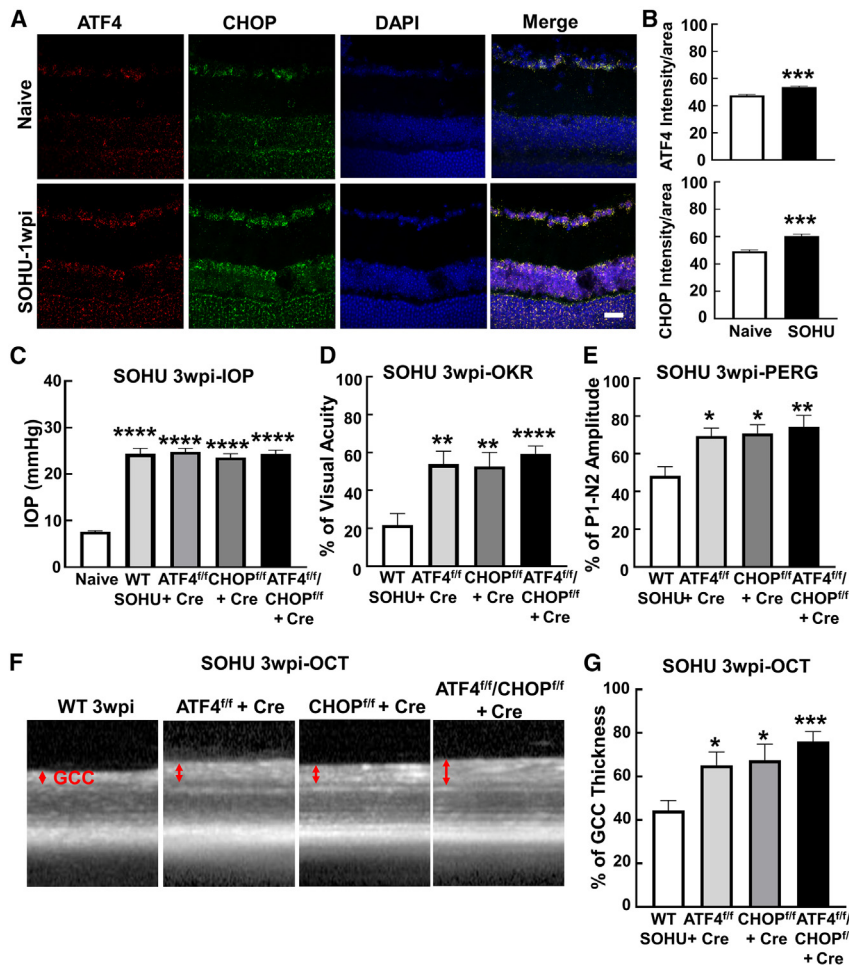


Figure 2. ATF4 and/or CHOP deletion preserve visual functions in SOHU glaucoma model

(A) Representative confocal images of retina cross-sections showing ATF4 (red) and CHOP (green) mRNA expression in GCL by ISH at 1wpi (1 week post SO injection). Scale bar, 20 μ m. (B) Quantification of mean fluorescence intensity of ATF4 and CHOP in GCL at 1wpi. $n = 5$. Data are presented as means \pm SEM. *** $p < 0.001$, two-tailed unpaired t test. (C) IOP measurements at 3wpi. Naive, $n = 15$; WT SOHU, $n = 15$; ATF4^{fl/fl}, $n = 12$; CHOP^{fl/fl}, $n = 9$; ATF4^{fl/fl}/CHOP^{fl/fl}, $n = 15$. (D) Visual acuity measured by OKR at 3wpi, represented as percentage of SOHU eyes compared to the sham contralateral control eyes. WT SOHU, $n = 15$; ATF4^{fl/fl}, $n = 12$; CHOP^{fl/fl}, $n = 9$; and ATF4^{fl/fl}/CHOP^{fl/fl}, $n = 15$. (E) Quantification of P1-N2 amplitude of PERG at 3wpi, represented as percentage of SOHU eyes compared to the sham contralateral control eyes. WT SOHU, $n = 15$; ATF4^{fl/fl}, $n = 12$; CHOP^{fl/fl}, $n = 9$; and ATF4^{fl/fl}/CHOP^{fl/fl}, $n = 15$. (F) Representative OCT images of mouse retina in living SOHU glaucoma animals at 3wpi. GCC (ganglion cell complex), including RNFL, GCL, and IPL layers, is indicated as double-end arrows. (G) Quantification of GCC thickness measured by OCT at 3wpi, represented as percentage of GCC thickness in the SOHU eyes compared to the sham contralateral control eyes. WT SOHU, $n = 15$; ATF4^{fl/fl}, $n = 12$; CHOP^{fl/fl}, $n = 9$; and ATF4^{fl/fl}/CHOP^{fl/fl}, $n = 15$. All the data are presented as means \pm SEM, * $p < 0.05$, ** $p < 0.01$, *** $p < 0.001$, **** $p < 0.0001$, one-way ANOVA with Tukey's multiple comparisons test.

achieves significant neuroprotection of RGCs and ONs in both traumatic ON injury and SOHU glaucoma models.

Topical application of ISRIB promotes both RGC soma and axon survival in SOHU glaucoma model

ISRIB is a small molecule blocker of the ATF4/CHOP pathway identified by high-throughput screening with a luciferase reporter driven by 5' UTR of ATF4 mRNA.⁵¹ We tested its effect on glaucomatous neurodegeneration. Topical application of ISRIB to retina by retrobulbar injection every 3 days had no effect on IOP elevation (Figure 4A), but it afforded consistent and significant neuroprotection of visual functions (Figures 4B and 4C), GCC thickness (Figures 4D and 4E), and RGC somata and axons (Figures 4F, 4G, and S3).

Inhibition of ATF4 downstream effector Gadd45a promotes neuroprotection in SOHU glaucoma model

Gadd45a is a potential downstream effector of the eIF2a-ATF4 branch of ER stress that mediates ER stress-induced cell death and muscle atrophy.^{44,52} We previously found that ONC injury induces Gadd45a expression in RGCs.²⁸ Gadd45a was also consistently upregulated in glaucomatous RGCs (Figures 5A and 5B). We have demon-

strated highly effective gene knockdown in RGCs by AAV-mSncg-mediated CRISPR.⁴⁵ Using a similar strategy to co-express Cas9 and Gadd45a gRNAs in mouse RGCs, we confirmed that

DISCUSSION

We previously demonstrated that germline deletion of CHOP or systemic administration of ATF4/CHOP inhibitors significantly protects RGC somata and axons.^{29,34} Here we investigated the autonomous effects of RGC-specific deletion of ATF4 and its downstream effector molecule CHOP in mouse optic neuropathy models. We demonstrated that neuronal ER stress, especially the ATF4-CHOP branch, plays a damaging autonomous role in traumatic and glaucomatous neurodegeneration. Consistent with the previous finding that ATF4 and CHOP act together to induce oxidative stress and apoptosis,⁴⁰ we confirmed that ATF4 and CHOP double KO synergistically promotes RGC and ON survival and preserves visual function in mouse ON crush and SOHU glaucoma models. Intriguingly, a recent study has extensively profiled the transcriptional targets of ATF4 and CHOP in RGCs and found that these two transcription factors regulate distinct molecular pathways.⁵³ Moreover, CHOP was found to inhibit ATF4 overactivation during mitochondrial stress, and deletion of CHOP may increase ATF4 expression.⁵⁴ Therefore, targeting

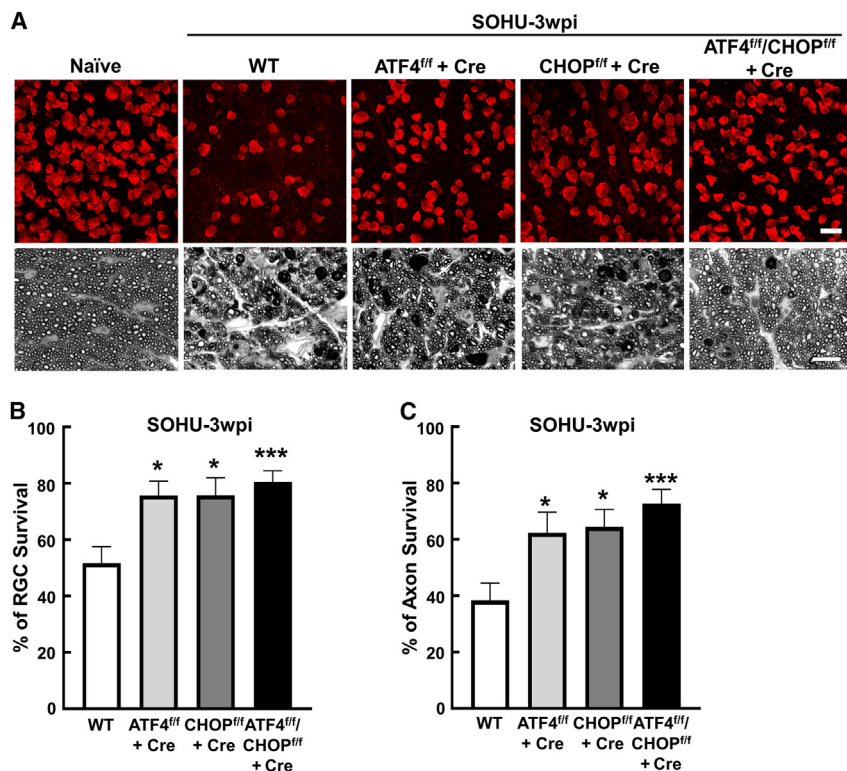


Figure 3. ATF4 and/or CHOP deletion promotes RGC soma and axon survival in SOHU glaucoma model

(A) Upper panel, representative confocal images of peripheral flat-mounted retinas showing surviving RBPMS-positive (red) RGCs at 3wpi. Scale bar, 20 μ m. Lower panel, light microscope images of semi-thin transverse sections of ON with PPD staining at 3wpi. Scale bar, 10 μ m. (B) Quantification of surviving RGC somata at 3wpi, represented as percentage of glaucomatous eyes compared to the sham contralateral control eyes. WT, n = 17; ATF4^{fl/fl}, n = 12; CHOP^{fl/fl}, n = 9; and ATF4^{fl/fl}/CHOP^{fl/fl}, n = 17. (C) Quantification of surviving RGCs axons at 3wpi, represented as percentage of glaucomatous eyes compared to the sham contralateral control eyes. WT, n = 17; ATF4^{fl/fl}, n = 12; CHOP^{fl/fl}, n = 9; and ATF4^{fl/fl}/CHOP^{fl/fl}, n = 17. Data are presented as means \pm SEM, *p < 0.05, ***p < 0.001, one-way ANOVA with Tukey's multiple comparisons test.

RGC-intrinsic ATF4 and CHOP simultaneously is a more promising neuroprotection strategy for optic neuropathies than inhibition of either alone. In addition, ATF4 activation has been found to be associated with AD,⁴¹ PD,⁴² and ALS.⁵⁵ Blocking the ATF4-CHOP pathway is, therefore, very likely to benefit multiple neurodegenerative diseases. Because recent findings suggest that astrocyte networks establish a connection between the glaucomatous and the contralateral eyes,^{56,57} it would be interesting to examine the responses of astrocytes in both eyes before and after ATF4/CHOP modulation.

Pharmacological small molecule modulators have been actively developed to target ER stress molecules.⁵⁸ Multiple FDA-approved drug compounds, such as adaptaquin, vortioxetine, trazodone, and dibenzoylmethane, have been found to be neuroprotective through blocking the ATF4/CHOP pathway.^{59–61} Recently, we identified three tricyclic drug compounds as general ER stress inhibitors through a small-scale high-throughput screening using a CHOP promoter-driven luciferase cell-based assay. Systemic administration of these agents showed considerable neuroprotection in mouse optic neuropathy models.³⁴ ISRIB is an effective chemical inhibitor of ATF4/CHOP by activating eIF2B.^{51,62,63} In addition to enhancing long-term memory,⁶⁴ it was found to be neuroprotective in mouse models of prion disease, ALS, and ONC.^{21,34,65,66} Here we performed retrobulbar injection of ISRIB to topically deliver it to the retinas and for the first time demonstrated that it provides significant neuroprotection in a mouse glaucoma model. However, ISRIB has poor solubility and is not suitable for human use. An ISRIB analog, 2BAct, has been developed with more favorable solu-

bility and pharmacokinetic properties.⁶⁷ It would be very interesting to test 2BAct in mouse optic neuropathy models. Further effort to develop neuroprotectants targeting ATF4/CHOP is certainly warranted.

CRISPR-mediated gene therapy directly inhibiting the ATF4/CHOP pathway is another promising therapeutic strategy for neuroprotection. We previously demonstrated RGC and ON protection in a mouse ONC model by AAV-mediated RGC-specific CRISPR knockdown of CHOP and SARM1.⁴⁵ In the current study, we used the same vectors with Gadd45a gRNAs, which also deliver significant neuroprotection in the SOHU glaucoma model. We recently generated a hyperCas12a, which enables highly efficient multiple gene editing simultaneously through a single poly-crRNA array driven by pol-II promoter in mouse retina *in vivo*.⁶⁸ This toolset will allow us to use AAV-hyperCas9 and corresponding crRNAs driven by RGC-specific promoters to develop synergistic neuroprotection gene therapy strategies that inhibit ATF4, CHOP, and their key downstream effectors, such as Gadd45a, specifically in RGCs.

Collectively, the results of the present study demonstrate that genetic and pharmacologic blocking of RGC-intrinsic ATF4 and CHOP protects injured and glaucomatous RGCs and ONs, suggesting that inhibiting the neuronal intrinsic ATF4/CHOP axis of ER stress is a promising neuroprotection strategy for neurodegeneration.

MATERIALS AND METHODS

Animals

C57BL/6J wild-type (WT) (#000664) and CHOP^{fl/fl} (#030816)⁴³ mice (7–9 weeks old) were purchased from Jackson Laboratories (Bar Harbor, Maine). ATF4^{fl/fl} mouse line was a gift from Dr. Sean Morrison's lab that was generated by Dr. Chris Adams lab.⁴⁴ All mice were

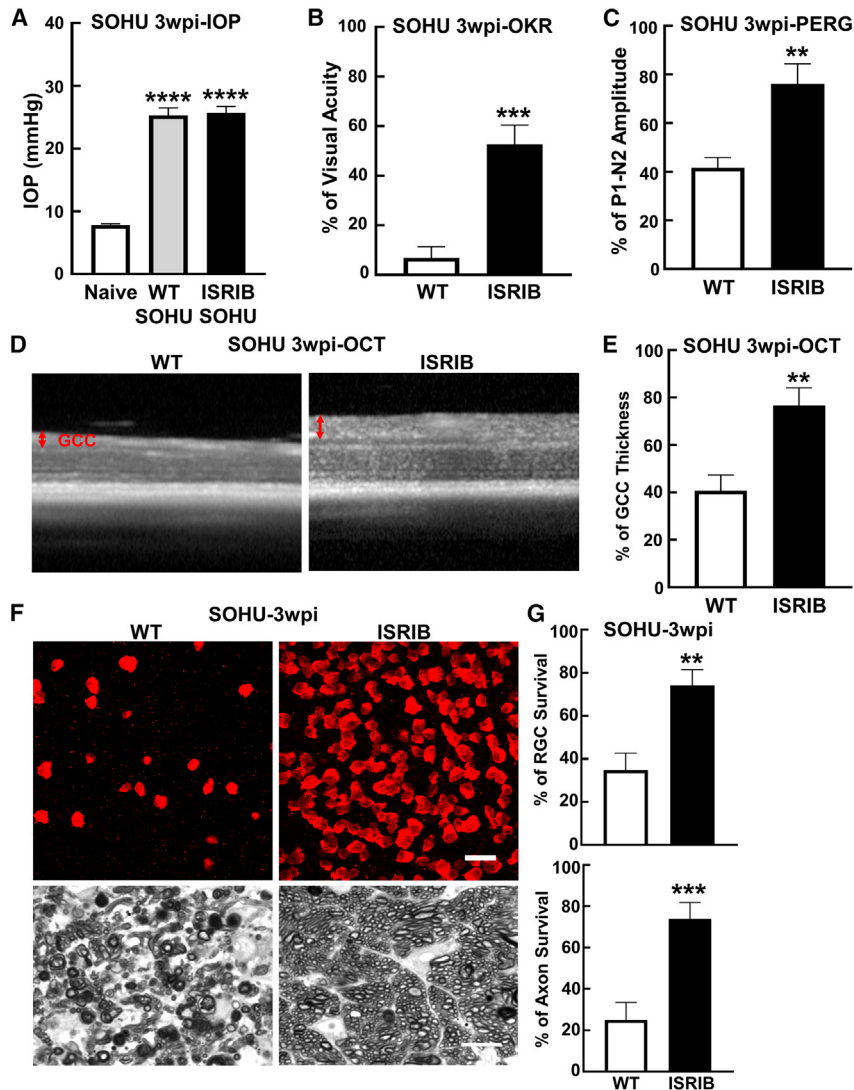


Figure 4. Retrolubar injection of ISRIB promotes RGC soma and axon survival and preserves visual function in SOHU glaucoma model

(A) IOP measurements at 3wpi. Naive, $n = 10$; WT SOHU, $n = 10$; ISRIB SOHU, $n = 12$. Data are presented as means \pm SEM, **** $p < 0.0001$, one-way ANOVA with Tukey's multiple comparisons test. (B) Visual acuity measured by OKR at 3wpi, represented as percentage of SOHU eyes compared to the sham contralateral control eyes. WT, $n = 10$; ISRIB, $n = 12$. Data are presented as means \pm SEM, *** $p < 0.001$, two-tailed unpaired t test. (C) Quantification of P1-N2 amplitude of PERG at 3wpi, represented as percentage of SOHU eyes compared to the sham contralateral control eyes. WT, $n = 10$; ISRIB, $n = 12$. Data are presented as means \pm SEM, ** $p < 0.01$, two-tailed unpaired t test. (D) Representative OCT images of mouse retina in living SOHU glaucoma animals at 3wpi. GCC is indicated as double-end arrows. (E) Quantification of GCC thickness measured by OCT at 3wpi, represented as percentage of GCC thickness in the SOHU eyes compared to the sham contralateral control eyes. WT, $n = 10$; ISRIB, $n = 12$. Data are presented as means \pm SEM, ** $p < 0.01$, two-tailed unpaired t test. (F) Upper panel, representative confocal images of peripheral flat-mounted retinas showing surviving RBPMS-positive (red) RGCs at 3wpi. Scale bar, 20 μ m. Lower panel, light microscope images of semi-thin transverse sections of ON with PPD staining at 3wpi. Scale bar, 10 μ m. (G) Quantification of surviving RGC somata and axons at 3wpi, represented as percentage of glaucomatous eyes compared to the sham contralateral control eyes. WT, $n = 10$; ISRIB, $n = 12$. Data are presented as means \pm SEM, ** $p < 0.01$, *** $p < 0.001$, two-tailed unpaired t test.

AAV production and intravitreal injection

The detailed procedure of AAV production has been described previously.^{29,45,69,70} The AAV titers were determined by real-time PCR and diluted to 1.5×10^{12} vector genome (vg)/ml. For intravitreal injection, mice were anesthetized with xylazine and ketamine based on their body weight (0.01 mg xylazine/g + 0.08 mg ketamine/g). A pulled and polished microcapillary needle was inserted into the peripheral retina just behind the ora serrata. Approximately 2 μ L of the vitreous was removed to allow injection of 2 μ L AAV into the vitreous chamber to achieve 3×10^9 vg/retina. The contralateral eyes were injected with 2 μ L control AAV2 as control.

ON crush model

ONC was performed 2 weeks following AAV injection.^{69–72} After anesthetization by intraperitoneal injection of Avertin (0.3 mg/g), the ON was exposed intraorbitally while care was taken not to damage the underlying ophthalmic artery and crushed with a jeweler's forceps (Dumont #5; Fine Science Tools, Foster City, California) for 5 s approximately 0.5 mm behind the eyeball. Neomycin eye ointment (Akorn, Somerset, New Jersey) was used to protect the cornea after surgery.

housed in standard cages on a 12-h light-dark cycle. All experimental procedures were performed in compliance with animal protocols approved by the IACUC (#32093) at Stanford University School of Medicine.

Constructs

The AAV2-mSncg-Cas9 and AAV2-hU6-sgRNAs-hU6-sgRNAs have been described before.⁴⁵ To maximize the KO efficiency, we designed two pairs (four gRNAs) targeting exon 2 and 3 of mouse Gadd45a. Pair 1: gRNA1: 5'-GGCACAGTACCACGT TATCG-3', gRNA2: 5'-CATTACGGTTCGGCGTGTACG-3'. Pair 2: gRNA3: 5'-CGAAGACGACGACCCGGGATG-3', gRNA4: 5'-CG CAGACCCCGGACCTGCAC-3'. The AAV vectors containing two pairs of gRNAs were mixed for packaging of AAV-Gadd45a gRNAs. AAV-Cas9 and AAV-Gadd45a gRNAs were intravitreally injected at ratio 2:1.

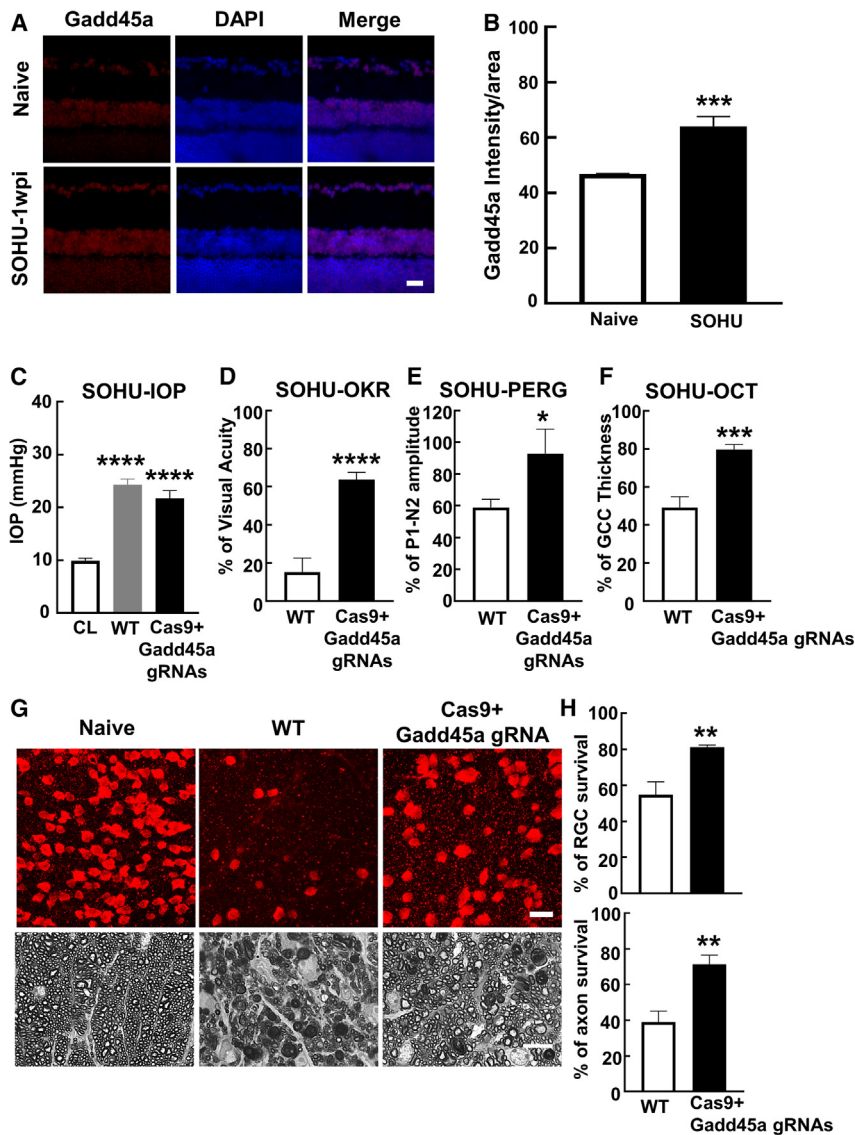


Figure 5. GADD45a knockdown (KD) promotes RGC soma and axon survival and preserves visual function in SOHU glaucoma model

(A) Representative confocal images of retina cross-sections showing GADD45a (red) mRNA expression in GCL by immunostaining at 1wpi. Scale bar, 20 μ m. (B) Quantification of mean fluorescence intensity of GADD45a in GCL. $n = 5$. All the data are presented as means \pm SEM. *** $p < 0.001$, two-tailed unpaired t test. (C) IOP measurements at 3wpi. Naive, $n = 13$; WT SOHU, $n = 13$; GADD45a KD, $n = 11$. Data are presented as means \pm SEM, **** $p < 0.0001$, one-way ANOVA with Tukey's multiple comparisons test. (D) Visual acuity measured by OKR at 3wpi, represented as percentage of SOHU eyes compared to the sham contralateral control eyes. WT, $n = 13$; GADD45a KD, $n = 10$. Data are presented as means \pm SEM, **** $p < 0.0001$, two-tailed unpaired t test. (E) Quantification of P1-N2 amplitude of PERG at 3wpi, represented as percentage of SOHU eyes compared to the sham contralateral control eyes. WT, $n = 13$; GADD45a KD, $n = 6$. Data are presented as means \pm SEM, * $p < 0.05$, two-tailed unpaired t test. (F) Quantification of GCC thickness measured by OCT at 3wpi, represented as percentage of GCC thickness in the SOHU eyes compared to the sham contralateral control eyes. WT, $n = 13$; GADD45a KD, $n = 9$. Data are presented as means \pm SEM, *** $p < 0.001$, two-tailed unpaired t test. (G) Upper panel, representative confocal images of peripheral flat-mounted retinas showing surviving RBPMS-positive (red) RGCs at 3wpi. Scale bar, 20 μ m. Lower panel, light microscope images of semi-thin transverse sections of ON with PPD staining at 3wpi. Scale bar, 10 μ m. (H) Quantification of surviving RGC somata and axons at 3wpi, represented as percentage of glaucomatous eyes compared to the sham contralateral control eyes. WT, $n = 13$; GADD45a KD, $n = 9$. Data are presented as means \pm SEM, ** $p < 0.01$, two-tailed unpaired t test.

SOHU glaucoma model and IOP measurement

SOHU mouse models and IOP measurement have been detailed before.^{46–48} In brief, mice were anesthetized by an intraperitoneal injection of Avertin (0.3 mg/g) and received the SO (Alcon Laboratories, 1,000 mPa s) injection at 9–10 weeks of age. Prior to injection, one drop of 0.5% proparacaine hydrochloride (Akorn, Somerset, New Jersey) was applied to the cornea to reduce its sensitivity during the procedure. A 32G needle was tunneled through the layers of the cornea at the superotemporal side close to the limbus to reach the anterior chamber without injuring the lens or iris. Following this entry, $\sim 2 \mu$ L silicone oil (1,000 mPa s, Silikon, Alcon Laboratories, Fort Worth, Texas) was injected slowly into the anterior chamber using a homemade sterile glass micropipette, until the oil droplet expanded to cover most areas of the iris (diameter ~ 1.8 – 2.2 mm). After the injection, veterinary antibiotic ointment (BNP ophthalmic

ointment, Vetropolycin, Dechra, Overland Park, Kansas) was applied to the surface of the injected eye. The contralateral control eyes received a mock injection with 2 μ L normal saline to the anterior chamber. Throughout the procedure, artificial tears (Systane Ultra Lubricant Eye Drops, Alcon Laboratories, Fort Worth, Texas) were applied to keep the cornea moist.

The detailed procedure for IOP measurement has been described before.^{46,47} The IOP of both eyes was measured by the TonoLab tonometer (Colonial Medical Supply, Espoo, Finland) according to product instructions under a sustained flow of isoflurane (3% isoflurane at 2 L/min mixed with oxygen) delivered to the nose by a special rodent nose cone (Xenotec, Rolla, Missouri). 1% Tropicamide Sterile Ophthalmic Solution (Akorn, Somerset, New Jersey) was applied three times at 3-min intervals to fully dilate the pupils (about 10 min) before taking measurements. During this procedure, artificial tears were applied to keep the cornea moist. Since IOP measurement requires pupil dilation, which essentially relieves ocular hypertension

during the period of pupil dilation, we only measure IOP 3 weeks after SO injection immediately before sacrificing the animals in the acute and severe ND (no dilation) SOHU model that we described before.⁴⁸

Fluorescent *in situ* hybridization with retina cross-sections

Fluorescent *in situ* hybridization was performed by using the RNA-scope Multiplex Fluorescent Detection Reagents V2 (Advanced Cell Diagnostics, ACD, Hayward, CA, USA) according to the manufacturer's instructions. RNAscope probe Mm-ATF4 (Cat No.405101) and Mm-Ddit3-C3 (Cat No.317661-C3) were purchased from ACD. Adult mice were perfused with ice-cold 4% PFA/PBS, and eyes were dissected out and fixed in 4% PFA/PBS at 4°C overnight. The eyes were dehydrated with increasing concentrations of sucrose solution (10%, 20%, and 30%) overnight before embedding in OCT on dry ice. Serial cross-sections (12 μm) were cut with a Leica cryostat and collected on Superfrost Plus Slides. The sections were pretreated with protease and then subjected to *in situ* hybridization with RNAscope Multiplex Fluorescent Detection Reagents V2 according to the manufacturer's instruction (ACD, Hayward, CA). Briefly, sections were hybridized with the probe solution, followed by amplification and probe detection using TSA plus fluorophores (AKOYA, Marlborough, MA, USA). The sections were mounted with Fluoromount-G (SouthernBiotech, Birmingham, AL, USA). Images were captured by a Zeiss LSM 880 confocal laser scanning microscope with 40×/1.0 Oil DIC (Carl Zeiss Microscopy, Thornwood, NY, USA). The quantification of ATF4 and CHOP fluorescence intensity was measured by NIH ImageJ after background correction. The results were calculated as the mean gray value (integrated density/retina area).

Immunohistochemistry of whole mounts and cross-sections of retina

The detailed procedures have been published before.^{30,45–48,71} Briefly, after perfusion fixation with 4% PFA in PBS, mice eyeballs and ONs were dissected out and post-fixed with 4% PFA for 2 h at room temperature. 30% sucrose was then used for cryoprotection of the tissues. Retinas were dissected out for whole-mount retina immunostaining. For cross-sections of retina, the eyeballs were embedded in tissue-tek OCT on dry ice for subsequent cryo-section with a Leica cryostat. The primary antibodies used for immunostaining were as follows: anti-RBPMS at 1:4,000 (Custom made at ProSci) and anti-GADD45a at 1:200 (Santa Cruz, sc-6850). Secondary antibodies were then applied (1:200; Jackson ImmunoResearch, West Grove, Pennsylvania) and incubated for 1 h at room temperature before mounting. The quantification of GADD45a fluorescence intensity was measured by NIH ImageJ. The results were calculated as the mean gray value (integrated density/area).

RGC counting

The detailed procedures have been published before.^{45–48,71,73} For peripheral RGC counting in the ON crush model, whole-mount retinas were immunostained with the RBPMS antibody, eight fields were sampled from peripheral regions of each retina using a 40× lens with a Zeiss M2 epifluorescence microscope, and RBPMS-positive RGCs were counted by Volocity software (Quorum Technologies).

For whole-retina RGC counting in the SOHU glaucoma model, the entire retina was imaged with the 20× objective lens of a Keyence fluorescence microscope (Figure S2A). Eight circles drawn by Concentric Circle plugin of NIH ImageJ were used to define the peripheral, middle, and inner areas of the retina. Multiple 100 × 100 μm counting frames were applied automatically by AxonCounter plugin of ImageJ to sample about 10% of each retina. The number of surviving RGCs in the sampled areas was manually counted by Cell Counter plugin of ImageJ. The percentage of RGC survival was calculated as the ratio of surviving RGC numbers in injured eyes compared to contralateral uninjured eyes. The investigators who counted the cells were masked to the treatment of the samples.

ON semi-thin sections and quantification of surviving axons

The detailed procedure of ON semi-thin section preparation and paraphenylenediamine (PPD) staining has been described previously.^{30,45,46,48,71} Briefly, ONs were post-fixed *in situ* with 2% glutaraldehyde and 2% PFA in 0.1 M PBS. Semi-thin (1-μm) cross-sections of the ON 2 mm distal to the eye (globe) were collected. After PPD staining, each ON was imaged by a 100× oil objective lens of a Keyence bright field microscope to cover the entire area of the ON without overlap. Multiple 10 × 10 μm counting frames were applied automatically by AxonCounter plugin of ImageJ to sample about 10% of each ON (Figure S2E).⁷⁴ The number of surviving axons in the sampled areas was manually identified and counted by Cell Counter plugin of ImageJ. The mean of the surviving axon number in the injured ON was compared to that in the contralateral control ON to yield a percentage of axon survival value. The investigators who counted the axons were masked to the treatment of the samples.

Spectral-domain optical coherence tomography imaging

The detailed procedure has been published previously.^{46,48,71} Briefly, after anesthetization (0.01 mg xylazine/g + 0.08 mg ketamine/g) and pupil dilation, the retina fundus images were captured with the Heidelberg Spectralis SLO/OCT system (Heidelberg Engineering, Germany). The mouse retina was scanned with the ring scan mode centered by the ON head under high-resolution mode (each B-scan consisted of 1,536 A-scans). The scanning ring had a fixed diameter of 160 μm, and the focal length was fixed at scale 37D. The ON head was always placed in the center of the ring, which allowed scanning the same area and same distance from the ON head to the ring of each eye. The GCC includes retinal nerve fiber layer (RNFL), ganglion cell layer (GCL), and inner plexiform layer (IPL). The average thickness of GCC around the ON head was measured manually with the aid of Heidelberg software. The investigators who measured the thickness of GCC were masked to the treatment of the samples.

Pattern electroretinogram recording

The detailed procedure has been published previously.^{46,48,71,75,76} Briefly, after anesthetization (0.01 mg xylazine/g + 0.08 mg ketamine/g) and pupil dilation, PERG of both eyes was recorded simultaneously with the Miami PERG system (Intelligent Hearing Systems, Miami, Florida) according to manufacturer's instructions. The pattern

remained at a contrast of 100% and a luminance of 800 cd/m², and it consisted of four cycles of black-gray elements, with a spatial frequency of 0.052 c/d. Two consecutive recordings of 200 traces were averaged to achieve one readout; each trace recorded up to 1,020 ms. The first positive peak in the waveform was designated as P1 and the second negative peak as N2. The amplitude was measured from P1 to N2.

Optokinetic tracking response (OKR)

The detailed procedure has been published previously.^{46,49,50} Briefly, mice were placed on a platform in the center of four 17-inch LCD computer monitors (Dell, Phoenix, AZ), with a video camera above the platform to capture the movement of the mouse. A rotating cylinder with vertical sine-wave grating was computed and projected to the four monitors by OptoMotry software (CerebralMechanics, Lethbridge, Alberta, Canada). The sine-wave grating, settled at 100% contrast and speed of 12° per second, provides a virtual reality environment to measure the spatial acuity (cycle/degree) of the left eye when rotated clockwise and the right eye when rotated counterclockwise. The maximum frequency (cycle/degree) that the mouse could track was identified and recorded by investigators masked to treatment.

Retrobulbar injection of ISRIB

ISRIB (MedChemExpress, Hy-12495) was freshly prepared with PBS before injection. The animals were anesthetized with a sustained flow of isoflurane (3% isoflurane at 2 L/min mixed with oxygen) delivered to the nose by a special rodent nose cone (Xenotec, Rolla, Missouri), and then the drug solutions (2 mM, 100 µL) were injected through the inferior palpebral subconjunctiva using a 30G disposable syringe one time every 3 days in the SOHU eyes. The contralateral control eyes received retrobulbar injection with 100 µL PBS.

Statistical analysis

GraphPad Prism 9 was used to generate graphs and for statistical analyses. Data are presented as means ± SEM. Student's t test was used for two groups comparison, and one-way ANOVA with post hoc test was used for multiple comparisons.

DATA AND CODE AVAILABILITY

All data generated or analyzed during this study are included in this article.

SUPPLEMENTAL INFORMATION

Supplemental information can be found online at <https://doi.org/10.1016/j.omtn.2023.07.015>.

ACKNOWLEDGMENTS

We thank Liang Liu for AAV production, Hu lab members, and Dr. Alan Tessler for the critical discussion and reading of the manuscript. Y.H. is supported by NIH grants EY024932, EY023295, EY028106, and EY032518 and grants from Glaucoma Research Foundation (CFC3), Chan Zuckerberg Initiative Neurodegeneration Collaborative Pairs Projects, Stanford SPARK program, and Stanford Center for Optic Disc Druse. F.F. is supported by National Natural Science Foundation of China (ref. 81500756), Natural Science Foundation

of Hunan (ref. 2023JJ10087), and Natural Science Foundation of Changsha (Reference: kq2208297). Portions of this work were supported by NIH grants R01EY025295, R01EY032159, VA merit CX001298, Children's Health Research Institute Award to Y.S., and R01DK113171, R01CA198103 and R01AG062190 to R.J.K. We are grateful for an unrestricted grant from Research to Prevent Blindness and NEI P30 EY026877 to the Department of Ophthalmology at Stanford University.

AUTHOR CONTRIBUTIONS

Y.H., F.F., and H.H. designed the experiments; F.F., P.L., H.H., X.F., and L.L. generated animal models and acquired histology and function analysis; L.Liu provided AAV production; Y.S. and R.J.K. provided reagents, mice, and reviewed the manuscript; Y.H., F.F., and H.H. prepared the manuscript with input from all authors.

DECLARATION OF INTERESTS

The authors have declared that no conflict of interest exists.

REFERENCES

- Walter, P., and Ron, D. (2011). The unfolded protein response: from stress pathway to homeostatic regulation. *Science* 334, 1081–1086. <https://doi.org/10.1126/science.1209038>.
- Hetz, C., Zhang, K., and Kaufman, R.J. (2020). Mechanisms, regulation and functions of the unfolded protein response. *Nat. Rev. Mol. Cell Biol.* 21, 421–438. <https://doi.org/10.1038/s41580-020-0250-z>.
- Li, S., Yang, L., Selzer, M.E., and Hu, Y. (2013). Neuronal endoplasmic reticulum stress in axon injury and neurodegeneration. *Ann. Neurol.* 74, 768–777. <https://doi.org/10.1002/ana.24005>.
- Valenzuela, V., Martínez, G., Duran-Aniotz, C., and Hetz, C. (2016). Gene therapy to target ER stress in brain diseases. *Brain Res.* 1648, 561–570. <https://doi.org/10.1016/j.brainres.2016.04.064>.
- Ghemrawi, R., and Khair, M. (2020). Endoplasmic Reticulum Stress and Unfolded Protein Response in Neurodegenerative Diseases. *Int. J. Mol. Sci.* 21, 6127. <https://doi.org/10.3390/ijms21176127>.
- Penas, C., Guzmán, M.S., Verdú, E., Forés, J., Navarro, X., and Casas, C. (2007). Spinal cord injury induces endoplasmic reticulum stress with different cell-type dependent response. *J. Neurochem.* 102, 1242–1255. <https://doi.org/10.1111/j.1471-4159.2007.04671.x>.
- Yamauchi, T., Sakurai, M., Abe, K., Matsumiya, G., and Sawa, Y. (2007). Impact of the endoplasmic reticulum stress response in spinal cord after transient ischemia. *Brain Res.* 1169, 24–33. <https://doi.org/10.1016/j.brainres.2007.06.093>.
- Mizukami, T., Orihashi, K., Herlambang, B., Takahashi, S., Hamaishi, M., Okada, K., and Sueda, T. (2010). Sodium 4-phenylbutyrate protects against spinal cord ischemia by inhibition of endoplasmic reticulum stress. *J. Vasc. Surg.* 52, 1580–1586. <https://doi.org/10.1016/j.jvs.2010.06.172>.
- Penas, C., Verdú, E., Asensio-Pinilla, E., Guzmán-Lenis, M.S., Herrando-Grabulosa, M., Navarro, X., and Casas, C. (2011). Valproate reduces CHOP levels and preserves oligodendrocytes and axons after spinal cord injury. *Neuroscience* 178, 33–44. <https://doi.org/10.1016/j.neuroscience.2011.01.012>.
- Ohri, S.S., Maddie, M.A., Zhao, Y., Qiu, M.S., Hetman, M., and Whitemore, S.R. (2011). Attenuating the endoplasmic reticulum stress response improves functional recovery after spinal cord injury. *Glia* 59, 1489–1502. <https://doi.org/10.1002/glia.21191>.
- Nakka, V.P., Gusain, A., and Raghuriv, R. (2010). Endoplasmic reticulum stress plays critical role in brain damage after cerebral ischemia/reperfusion in rats. *Neurotox. Res.* 17, 189–202. <https://doi.org/10.1007/s12640-009-9110-5>.
- Yuan, Y., Guo, Q., Ye, Z., Pingping, X., Wang, N., and Song, Z. (2011). Ischemic post-conditioning protects brain from ischemia/reperfusion injury by attenuating

- endoplasmic reticulum stress-induced apoptosis through PI3K-Akt pathway. *Brain Res.* 1367, 85–93. <https://doi.org/10.1016/j.brainres.2010.10.017>.
13. Krajewska, M., Xu, L., Xu, W., Krajewski, S., Kress, C.L., Cui, J., Yang, L., Irie, F., Yamaguchi, Y., Lipton, S.A., and Reed, J.C. (2011). Endoplasmic reticulum protein BI-1 modulates unfolded protein response signaling and protects against stroke and traumatic brain injury. *Brain Res.* 1370, 227–237. <https://doi.org/10.1016/j.brainres.2010.11.015>.
 14. Casas-Tinto, S., Zhang, Y., Sanchez-Garcia, J., Gomez-Velazquez, M., Rincon-Limas, D.E., and Fernandez-Funez, P. (2011). The ER stress factor XBP1s prevents amyloid-beta neurotoxicity. *Hum. Mol. Genet.* 20, 2144–2160. <https://doi.org/10.1093/hmg/ddr100>.
 15. Ma, T., Trinh, M.A., Wexler, A.J., Bourbon, C., Gatti, E., Pierre, P., Cavener, D.R., and Klann, E. (2013). Suppression of eIF2alpha kinases alleviates Alzheimer's disease-related plasticity and memory deficits. *Nat. Neurosci.* 16, 1299–1305. <https://doi.org/10.1038/nn.3486>.
 16. Sado, M., Yamasaki, Y., Iwanaga, T., Onaka, Y., Ibuki, T., Nishihara, S., Mizuguchi, H., Momota, H., Kishibuchi, R., Hashimoto, T., et al. (2009). Protective effect against Parkinson's disease-related insults through the activation of XBP1. *Brain Res.* 1257, 16–24. <https://doi.org/10.1016/j.brainres.2008.11.104>.
 17. Valdés, P., Mercado, G., Vidal, R.L., Molina, C., Parsons, G., Court, F.A., Martinez, A., Galleguillos, D., Armentano, D., Schneider, B.L., and Hetz, C. (2014). Control of dopaminergic neuron survival by the unfolded protein response transcription factor XBP1. *Proc. Natl. Acad. Sci. USA* 111, 6804–6809. <https://doi.org/10.1073/pnas.1321845111>.
 18. Saxena, S., Cabuy, E., and Caroni, P. (2009). A role for motoneuron subtype-selective ER stress in disease manifestations of FALS mice. *Nat. Neurosci.* 12, 627–636. <https://doi.org/10.1038/nn.2297>.
 19. Moreno, J.A., Halliday, M., Molloy, C., Radford, H., Verity, N., Axten, J.M., Ortori, C.A., Willis, A.E., Fischer, P.M., Barrett, D.A., and Mallucci, G.R. (2013). Oral treatment targeting the unfolded protein response prevents neurodegeneration and clinical disease in prion-infected mice. *Sci. Transl. Med.* 5, 206ra138. <https://doi.org/10.1126/scitranslmed.3006767>.
 20. Moreno, J.A., Radford, H., Peretti, D., Steinert, J.R., Verity, N., Martin, M.G., Halliday, M., Morgan, J., Dinsdale, D., Ortori, C.A., et al. (2012). Sustained translational repression by eIF2alpha-P mediates prion neurodegeneration. *Nature* 485, 507–511. <https://doi.org/10.1038/nature11058>.
 21. Halliday, M., Radford, H., Sekine, Y., Moreno, J., Verity, N., le Quesne, J., Ortori, C.A., Barrett, D.A., Fromont, C., Fischer, P.M., et al. (2015). Partial restoration of protein synthesis rates by the small molecule ISRIB prevents neurodegeneration without pancreatic toxicity. *Cell Death Dis.* 6, e1672. <https://doi.org/10.1038/cddis.2015.49>.
 22. Doh, S.H., Kim, J.H., Lee, K.M., Park, H.Y., and Park, C.K. (2010). Retinal ganglion cell death induced by endoplasmic reticulum stress in a chronic glaucoma model. *Brain Res.* 1308, 158–166. <https://doi.org/10.1016/j.brainres.2009.10.025>.
 23. Boriushkin, E., Wang, J.J., Li, J., Jing, G., Seigel, G.M., and Zhang, S.X. (2015). Identification of p58IPK as a novel neuroprotective factor for retinal neurons. *Invest. Ophthalmol. Vis. Sci.* 56, 1374–1386. <https://doi.org/10.1167/iov.14-15196>.
 24. Chan, P., Stolz, J., Kohl, S., Chiang, W.C., and Lin, J.H. (2016). Endoplasmic reticulum stress in human photoreceptor diseases. *Brain Res.* 1648, 538–541. <https://doi.org/10.1016/j.brainres.2016.04.021>.
 25. Kohl, S., Zobor, D., Chiang, W.C., Weisschuh, N., Staller, J., Gonzalez Menendez, I., Chang, S., Beck, S.C., Garcia Garrido, M., Sothilingam, V., et al. (2015). Mutations in the unfolded protein response regulator ATF6 cause the cone dysfunction disorder achromatopsia. *Nat. Genet.* 47, 757–765. <https://doi.org/10.1038/ng.3319>.
 26. Lin, J.H., Li, H., Yasumura, D., Cohen, H.R., Zhang, C., Panning, B., Shokat, K.M., Lavail, M.M., and Walter, P. (2007). IRE1 signaling affects cell fate during the unfolded protein response. *Science* 318, 944–949. <https://doi.org/10.1126/science.1146361>.
 27. Ghosh, R., Wang, L., Wang, E.S., Perera, B.G.K., Igbaria, A., Morita, S., Prado, K., Thamsen, M., Caswell, D., Macias, H., et al. (2014). Allosteric inhibition of the IRE1alpha RNase preserves cell viability and function during endoplasmic reticulum stress. *Cell* 158, 534–548. <https://doi.org/10.1016/j.cell.2014.07.002>.
 28. Hu, Y., Park, K.K., Yang, L., Wei, X., Yang, Q., Cho, K.S., Thielen, P., Lee, A.H., Cartoni, R., Glimcher, L.H., et al. (2012). Differential effects of unfolded protein response pathways on axon injury-induced death of retinal ganglion cells. *Neuron* 73, 445–452. <https://doi.org/10.1016/j.neuron.2011.11.026>.
 29. Yang, L., Li, S., Miao, L., Huang, H., Liang, F., Teng, X., Xu, L., Wang, Q., Xiao, W., Ridder, W.H., 3rd, et al. (2016). Rescue of Glaucomatous Neurodegeneration by Differentially Modulating Neuronal Endoplasmic Reticulum Stress Molecules. *J. Neurosci.* 36, 5891–5903. <https://doi.org/10.1523/JNEUROSCI.3709-15.2016>.
 30. Huang, H., Miao, L., Liang, F., Liu, X., Xu, L., Teng, X., Wang, Q., Ridder, W.H., 3rd, Shindler, K.S., Sun, Y., and Hu, Y. (2017). Neuroprotection by eIF2alpha-CHOP inhibition and XBP-1 activation in EAE/optic neuritis. *Cell Death Dis.* 8. <https://doi.org/10.1038/cddis.2017.329>.
 31. Zinszner, H., Kuroda, M., Wang, X., Batchvarova, N., Lightfoot, R.T., Remotti, H., Stevens, J.L., and Ron, D. (1998). CHOP is implicated in programmed cell death in response to impaired function of the endoplasmic reticulum. *Genes Dev.* 12, 982–995. <https://doi.org/10.1101/gad.12.7.982>.
 32. Silva, R.M., Ries, V., Oo, T.F., Yarygina, O., Jackson-Lewis, V., Ryu, E.J., Lu, P.D., Marciniak, S.J., Ron, D., Przedborski, S., et al. (2005). CHOP/GADD153 is a mediator of apoptotic death in substantia nigra dopamine neurons in an in vivo neurotoxin model of parkinsonism. *J. Neurochem.* 95, 974–986. <https://doi.org/10.1111/j.1471-4159.2005.03428.x>.
 33. Song, B., Scheuner, D., Ron, D., Pennathur, S., and Kaufman, R.J. (2008). Chop deletion reduces oxidative stress, improves beta cell function, and promotes cell survival in multiple mouse models of diabetes. *J. Clin. Invest.* 118, 3378–3389. <https://doi.org/10.1172/JCI34587>.
 34. Chen, W., Liu, P., Liu, D., Huang, H., Feng, X., Fang, F., Li, L., Wu, J., Liu, L., Solow-Cordero, D.E., and Hu, Y. (2022). Maptroline restores ER homeostasis and rescues neurodegeneration via Histamine Receptor H1 inhibition in retinal ganglion cells. *Nat. Commun.* 13, 6796. <https://doi.org/10.1038/s41467-022-34682-y>.
 35. Hu, Y. (2016). Axon injury induced endoplasmic reticulum stress and neurodegeneration. *Neural Regen. Res.* 11, 1557–1559. <https://doi.org/10.4103/1673-5374.193225>.
 36. McCullough, K.D., Martindale, J.L., Klotz, L.O., Aw, T.Y., and Holbrook, N.J. (2001). Gadd153 sensitizes cells to endoplasmic reticulum stress by down-regulating Bcl2 and perturbing the cellular redox state. *Mol. Cell Biol.* 21, 1249–1259. <https://doi.org/10.1128/MCB.21.4.1249-1259.2001>.
 37. Puthalakath, H., O'Reilly, L.A., Gunn, P., Lee, L., Kelly, P.N., Huntington, N.D., Hughes, P.D., Michalak, E.M., McKimm-Breschkin, J., Motoyama, N., et al. (2007). ER stress triggers apoptosis by activating BH3-only protein Bim. *Cell* 129, 1337–1349. <https://doi.org/10.1016/j.cell.2007.04.027>.
 38. Galehdar, Z., Swan, P., Fuerth, B., Callaghan, S.M., Park, D.S., and Cregan, S.P. (2010). Neuronal apoptosis induced by endoplasmic reticulum stress is regulated by ATF4-CHOP-mediated induction of the Bcl-2 homology 3-only member PUMA. *J. Neurosci.* 30, 16938–16948. <https://doi.org/10.1523/JNEUROSCI.1598-10.2010>.
 39. Lu, M., Lawrence, D.A., Marsters, S., Acosta-Alvear, D., Kimmig, P., Mendez, A.S., Paton, A.W., Paton, J.C., Walter, P., and Ashkenazi, A. (2014). Opposing unfolded-protein-response signals converge on death receptor 5 to control apoptosis. *Science* 345, 98–101. <https://doi.org/10.1126/science.1254312>.
 40. Han, J., Back, S.H., Hur, J., Lin, Y.H., Gildersleeve, R., Shan, J., Yuan, C.L., Krokowski, D., Wang, S., Hatzoglou, M., et al. (2013). ER-stress-induced transcriptional regulation increases protein synthesis leading to cell death. *Nat. Cell Biol.* 15, 481–490. <https://doi.org/10.1038/ncb2738>.
 41. Baleriola, J., Walker, C.A., Jean, Y.Y., Crary, J.F., Troy, C.M., Nagy, P.L., and Hengst, U. (2014). Axonally synthesized ATF4 transmits a neurodegenerative signal across brain regions. *Cell* 158, 1159–1172. <https://doi.org/10.1016/j.cell.2014.07.001>.
 42. Demmings, M.D., Tennyson, E.C., Petroff, G.N., Tarnowski-Garner, H.E., and Cregan, S.P. (2021). Activating transcription factor-4 promotes neuronal death induced by Parkinson's disease neurotoxins and alpha-synuclein aggregates. *Cell Death Differ.* 28, 1627–1643. <https://doi.org/10.1038/s41418-020-00688-6>.
 43. Zhou, A.X., Wang, X., Lin, C.S., Han, J., Yong, J., Nadolski, M.J., Borén, J., Kaufman, R.J., and Tabas, I. (2015). C/EBP-Homologous Protein (CHOP) in Vascular Smooth Muscle Cells Regulates Their Proliferation in Aortic Explants and Atherosclerotic Lesions. *Circ. Res.* 116, 1736–1743. <https://doi.org/10.1161/CIRCRESAHA.116.305602>.
 44. Ebert, S.M., Dyle, M.C., Kunkel, S.D., Bullard, S.A., Bongers, K.S., Fox, D.K., Dierdorff, J.M., Foster, E.D., and Adams, C.M. (2012). Stress-induced skeletal muscle

- Gadd45a expression reprograms myonuclei and causes muscle atrophy. *J. Biol. Chem.* 287, 27290–27301. <https://doi.org/10.1074/jbc.M112.374777>.
45. Wang, Q., Zhuang, P., Huang, H., Li, L., Liu, L., Webber, H.C., Dalal, R., Siew, L., Fligor, C.M., Chang, K.C., et al. (2020). Mouse gamma-Synuclein Promoter-Mediated Gene Expression and Editing in Mammalian Retinal Ganglion Cells. *J. Neurosci.* 40, 3896–3914. <https://doi.org/10.1523/JNEUROSCI.0102-20.2020>.
 46. Zhang, J., Li, L., Huang, H., Fang, F., Webber, H.C., Zhuang, P., Liu, L., Dalal, R., Tang, P.H., Mahajan, V.B., et al. (2019). Silicone oil-induced ocular hypertension and glaucomatous neurodegeneration in mouse. *Elife* 8, e45881. <https://doi.org/10.7554/eLife.45881>.
 47. Zhang, J., Fang, F., Li, L., Huang, H., Webber, H.C., Sun, Y., Mahajan, V.B., and Hu, Y. (2019). A Reversible Silicon Oil-Induced Ocular Hypertension Model in Mice. *J. Vis. Exp.* 153. <https://doi.org/10.3791/60409>.
 48. Fang, F., Zhang, J., Zhuang, P., Liu, P., Li, L., Huang, H., Webber, H.C., Xu, Y., Liu, L., Dalal, R., et al. (2021). Chronic mild and acute severe glaucomatous neurodegeneration derived from silicone oil-induced ocular hypertension. *Sci. Rep.* 11, 9052. <https://doi.org/10.1038/s41598-021-88690-x>.
 49. Prusky, G.T., Alam, N.M., Beekman, S., and Douglas, R.M. (2004). Rapid quantification of adult and developing mouse spatial vision using a virtual optomotor system. *Invest. Ophthalmol. Vis. Sci.* 45, 4611–4616. <https://doi.org/10.1167/iovs.04-0541>.
 50. Douglas, R.M., Alam, N.M., Silver, B.D., McGill, T.J., Tschetter, W.W., and Prusky, G.T. (2005). Independent visual threshold measurements in the two eyes of freely moving rats and mice using a virtual-reality optokinetic system. *Vis. Neurosci.* 22, 677–684. <https://doi.org/10.1017/S0952523805225166>.
 51. Sidrauski, C., Acosta-Alvarez, D., Khoutorsky, A., Vedantham, P., Hearn, B.R., Li, H., Gamache, K., Gallagher, C.M., Ang, K.K.H., Wilson, C., et al. (2013). Pharmacological brake-release of mRNA translation enhances cognitive memory. *Elife* 2, e00498. <https://doi.org/10.7554/eLife.00498>.
 52. Lee, D., Hokinson, D., Park, S., Elvira, R., Kusuma, F., Lee, J.M., Yun, M., Lee, S.G., and Han, J. (2019). ER Stress Induces Cell Cycle Arrest at the G2/M Phase Through eIF2alpha Phosphorylation and GADD45alpha. *Int. J. Mol. Sci.* 20, 6309. <https://doi.org/10.3390/ijms20246309>.
 53. Tian, F., Cheng, Y., Zhou, S., Wang, Q., Monavarfeshani, A., Gao, K., Jiang, W., Kawaguchi, R., Wang, Q., Tang, M., et al. (2022). Core transcription programs controlling injury-induced neurodegeneration of retinal ganglion cells. *Neuron* 110, 2607–2624.e8. <https://doi.org/10.1016/j.neuron.2022.06.003>.
 54. Kaspar, S., Oertlin, C., Szczepanowska, K., Kukat, A., Senft, K., Lucas, C., Brodesser, S., Hatzoglou, M., Larsson, O., Topisirovic, I., and Trifunovic, A. (2021). Adaptation to mitochondrial stress requires CHOP-directed tuning of. *Sci. Adv.* 7, eabf0971. <https://doi.org/10.1126/sciadv.abf0971>.
 55. Matus, S., Lopez, E., Valenzuela, V., Nassif, M., and Hetz, C. (2013). Functional contribution of the transcription factor ATF4 to the pathogenesis of amyotrophic lateral sclerosis. *PLoS One* 8, e66672. <https://doi.org/10.1371/journal.pone.0066672>.
 56. Cooper, M.L., Pasini, S., Lambert, W.S., D'Alessandro, K.B., Yao, V., Risner, M.L., and Calkins, D.J. (2020). Redistribution of metabolic resources through astrocyte networks mitigates neurodegenerative stress. *Proc. Natl. Acad. Sci. USA* 117, 18810–18821. <https://doi.org/10.1073/pnas.2009425117>.
 57. McGrady, N.R., Boal, A.M., Risner, M.L., Taiel, M., Sahel, J.A., and Calkins, D.J. (2023). Ocular stress enhances contralateral transfer of lenadogene nolparvovec gene therapy through astrocyte networks. *Mol. Ther.* 31, 2005–2013. <https://doi.org/10.1016/j.ymthe.2023.03.035>.
 58. Hetz, C., Axten, J.M., and Patterson, J.B. (2019). Pharmacological targeting of the unfolded protein response for disease intervention. *Nat. Chem. Biol.* 15, 764–775. <https://doi.org/10.1038/s41589-019-0326-2>.
 59. Aimé, P., Karuppagounder, S.S., Rao, A., Chen, Y., Burke, R.E., Ratan, R.R., and Greene, L.A. (2020). The drug adaptaquin blocks ATF4/CHOP-dependent pro-death Trib3 induction and protects in cellular and mouse models of Parkinson's disease. *Neurobiol. Dis.* 136, 104725. <https://doi.org/10.1016/j.nbd.2019.104725>.
 60. Emam, A.M., Saad, M.A., Ahmed, N.A., and Zaki, H.F. (2021). Vortioxetine mitigates neuronal damage by restricting PERK/eIF2alpha/ATF4/CHOP signaling pathway in rats subjected to focal cerebral ischemia-reperfusion. *Life Sci.* 283, 119865. <https://doi.org/10.1016/j.lfs.2021.119865>.
 61. Halliday, M., Radford, H., Zents, K.A.M., Molloy, C., Moreno, J.A., Verity, N.C., Smith, E., Ortori, C.A., Barrett, D.A., Bushell, M., and Mallucci, G.R. (2017). Repurposed drugs targeting eIF2 α -P-mediated translational repression prevent neurodegeneration in mice. *Brain* 140, 1768–1783. <https://doi.org/10.1093/brain/awx074>.
 62. Sekine, Y., Zyryanova, A., Crespillo-Casado, A., Fischer, P.M., Harding, H.P., and Ron, D. (2015). Stress responses. Mutations in a translation initiation factor identify the target of a memory-enhancing compound. *Science* 348, 1027–1030. <https://doi.org/10.1126/science.aaa6986>.
 63. Sidrauski, C., Tsai, J.C., Kampmann, M., Hearn, B.R., Vedantham, P., Jaishankar, P., Sokabe, M., Mendez, A.S., Newton, B.W., Tang, E.L., et al. (2015). Pharmacological dimerization and activation of the exchange factor eIF2B antagonizes the integrated stress response. *Elife* 4, e07314. <https://doi.org/10.7554/eLife.07314>.
 64. Costa-Mattioli, M., and Walter, P. (2020). The integrated stress response: From mechanism to disease. *Science* 368, eaat5314. <https://doi.org/10.1126/science.aat5314>.
 65. Bugallo, R., Marlin, E., Baltanás, A., Toledo, E., Ferrero, R., Vinuesa-Gavilanes, R., Larrea, L., Arrasate, M., and Aragón, T. (2020). Fine tuning of the unfolded protein response by ISRIB improves neuronal survival in a model of amyotrophic lateral sclerosis. *Cell Death Dis.* 11, 397. <https://doi.org/10.1038/s41419-020-2601-2>.
 66. Larhammar, M., Huntwork-Rodriguez, S., Jiang, Z., Solano, H., Sengupta Ghosh, A., Wang, B., Kaminker, J.S., Huang, K., Eastham-Anderson, J., Siu, M., et al. (2017). Dual leucine zipper kinase-dependent PERK activation contributes to neuronal degeneration following insult. *Elife* 6, e20725. <https://doi.org/10.7554/eLife.20725>.
 67. Wong, Y.L., LeBon, L., Basso, A.M., Kohlhaas, K.L., Nikkel, A.L., Robb, H.M., Donnelly-Roberts, D.L., Prakash, J., Swensen, A.M., Rubinstein, N.D., et al. (2019). eIF2B activator prevents neurological defects caused by a chronic integrated stress response. *Elife* 8, e42940. <https://doi.org/10.7554/eLife.42940>.
 68. Guo, L.Y., Bian, J., Davis, A.E., Liu, P., Kempton, H.R., Zhang, X., Chemparathy, A., Gu, B., Lin, X., Rane, D.A., et al. (2022). Multiplexed genome regulation in vivo with hyper-efficient Cas12a. *Nat. Cell Biol.* 24, 590–600. <https://doi.org/10.1038/s41556-022-00870-7>.
 69. Yang, L., Miao, L., Liang, F., Huang, H., Teng, X., Li, S., Nuriddinov, J., Selzer, M.E., and Hu, Y. (2014). The mTORC1 effectors S6K1 and 4E-BP play different roles in CNS axon regeneration. *Nat. Commun.* 5, 5416. <https://doi.org/10.1038/ncomms6416>.
 70. Miao, L., Yang, L., Huang, H., Liang, F., Ling, C., and Hu, Y. (2016). mTORC1 is necessary but mTORC2 and GSK3beta are inhibitory for AKT3-induced axon regeneration in the central nervous system. *Elife* 5, e14908. <https://doi.org/10.7554/eLife.14908>.
 71. Li, L., Huang, H., Fang, F., Liu, L., Sun, Y., and Hu, Y. (2020). Longitudinal Morphological and Functional Assessment of RGC Neurodegeneration After Optic Nerve Crush in Mouse. *Front. Cell. Neurosci.* 14, 109. <https://doi.org/10.3389/fncel.2020.00109>.
 72. Huang, H., Miao, L., Yang, L., Liang, F., Wang, Q., Zhuang, P., Sun, Y., and Hu, Y. (2019). AKT-dependent and -independent pathways mediate PTEN deletion-induced CNS axon regeneration. *Cell Death Dis.* 10, 203. <https://doi.org/10.1038/s41419-018-1289-z>.
 73. Liu, P., Chen, W., Jiang, H., Huang, H., Liu, L., Fang, F., Li, L., Feng, X., Liu, D., Dalal, R., et al. (2023). Differential effects of SARM1 inhibition in traumatic glaucoma and EAE optic neuropathies. *Mol. Ther. Nucleic Acids* 32, 13–27. <https://doi.org/10.1016/j.omtn.2023.02.029>.
 74. Koschade, S.E., Koch, M.A., Braunger, B.M., and Tamm, E.R. (2019). Efficient determination of axon number in the optic nerve: A stereological approach. *Exp. Eye Res.* 186, 107710. <https://doi.org/10.1016/j.exer.2019.107710>.
 75. Chou, T.H., Bohorquez, J., Toft-Nielsen, J., Ozdamar, O., and Porciatti, V. (2014). Robust mouse pattern electroretinograms derived simultaneously from each eye using a common snout electrode. *Invest. Ophthalmol. Vis. Sci.* 55, 2469–2475. <https://doi.org/10.1167/iovs.14-13943>.
 76. Porciatti, V. (2015). Electrophysiological assessment of retinal ganglion cell function. *Exp. Eye Res.* 141, 164–170. <https://doi.org/10.1016/j.exer.2015.05.008>.